PREPRINT 517

JULY 2021

A unified surface-gradient and hydrostatic reconstruction scheme for the shallow water equations

Guoxian Chen[a,b] and Sebastian Noelle[c]

Institut für Geometrie und Praktische Mathematik
Templergraben 55, 52062 Aachen, Germany

a School of Mathematics and Statistics, Wuhan University, Wuhan, 430072, P.R. China.
b Computational Science Hubei Key Laboratory, Wuhan University, Wuhan, 430072, P.R. China.
c Institute for Geometry and Practical Mathematics, RWTH Aachen University, Templergraben 55, 52062, Aachen, Germany.

A unified surface-gradient and hydrostatic reconstruction scheme for the shallow water equations

Guoxian Chen[a,b], Sebastian Noelle[c]

[a]School of Mathematics and Statistics, Wuhan University, Wuhan, 430072, P.R. China.
[b]Computational Science Hubei Key Laboratory, Wuhan University, Wuhan, 430072, P.R. China.
[c]Institute for Geometry and Practical Mathematics, RWTH Aachen University, Templergraben 55, 52062, Aachen, Germany.

Abstract

We propose a new second-order accurate hydrostatic reconstruction scheme for the Saint-Venant system. Such a scheme needs to overcome several difficulties: besides the well-known issues of positivity and well-balancing there is also the difficulty of unphysical reflections from bottom reconstructions which create artificial steps. We address all of these problems at once by changing the logic of the reconstruction of the bottom, the water depth and the water surface level. Notably, our bottom reconstruction is continuous across cell interfaces and remains unchanged during the computation, except if the original topography has a jump, or if a wet-dry front passes through a cell. Only in these exceptional cases we apply the new discontinuous bottom approximation and compute the residual via the subcell hydrostatic reconstruction method. The scheme gives excellent results in one and two space dimensions. To highlight the novel reconstruction of bottom and water surface, we call the scheme *bottom-surface-gradient method* (BSGM).

Keywords: Saint-Venant system, well-balanced property, positivity preserving property, subcell hydrostatic reconstruction, bottom-surface-gradient method, maximum-minimum property.
2010 MSC: 76M12, 35L65

1. Introduction

Incompressible free surface flows occur between a piecewise continuous bottom topography

$$\mathcal{B} := \{(x, y, z)|\ (x, y) \in \Omega,\ z = b(x, y)\}, \tag{1.1}$$

and a water surface

$$\mathcal{W}(t) := \{(x, y, z)|\ (x, y) \in \Omega,\ z = w(x, y, t)\} \tag{1.2}$$

over some two-dimensional domain Ω and at a fixed time $t \in [0, T]$. The discrete analogues of these two surfaces will play a key role in the derivation of the bottom-surface-gradient method.

Email addresses: gxchen.math@whu.edu.cn (Guoxian Chen), noelle@igpm.rwth-aachen.de (Sebastian Noelle)

At each instance in time, the three-dimensional flow domain $\widehat{\Omega}(t)$ is divided into a wet and a dry part,

$$\widehat{\Omega}(t) = \widehat{\Omega}_{\text{wet}}(t) \cup \widehat{\Omega}_{\text{dry}}(t), \tag{1.3}$$

where

$$\widehat{\Omega}_{\text{wet}}(t) := \{(x, y, z) |\ b(x, y) < z < w(x, y, t)\}, \tag{1.4}$$

$$\widehat{\Omega}_{\text{dry}}(t) := \{(x, y, z) |\ b(x, y) = z = w(x, y, t)\}. \tag{1.5}$$

Let $\Omega_{\text{wet}}(t)$ respectively $\Omega_{\text{dry}}(t)$ be the projections of $\widehat{\Omega}_{\text{wet}}(t)$ respectively $\widehat{\Omega}_{\text{dry}}(t)$ onto Ω, and let

$$\Gamma(t) := \text{closure}\big(\Omega_{\text{wet}}(t)\big) \cap \text{closure}\big(\Omega_{\text{dry}}(t)\big) \tag{1.6}$$

be the wet-dry front. Furthermore, let

$$\overline{\Omega} := \{(x, y, t) \in \Omega \times (0, T)\} \tag{1.7}$$

$$\overline{\Omega}_{\text{wet}} := \{(x, y, t) \in \overline{\Omega} \mid (x, y) \in \Omega_{\text{wet}}(t)\} \tag{1.8}$$

$$\overline{\Omega}_{\text{dry}} := \{(x, y, t) \in \overline{\Omega} \mid (x, y) \in \Omega_{\text{dry}}(t)\} \tag{1.9}$$

be the space-time domain together with its wet and dry parts. Assuming uniform density of the water, kinematic boundary conditions, hydrostatic pressure, constant vertical velocity profiles, and taking the depth-average of the incompressible Euler equations, one arrives at the two-dimensional Saint-Venant equations [1, 2]

$$\left.\begin{array}{rcl} \partial_t h + \partial_x(hu) + \partial_y(hv) & = & 0 \\ \partial_t(hu) + \partial_x(hu^2 + \frac{1}{2}gh^2) + \partial_y(huv) & = & -gh\partial_x b \\ \partial_t(hv) + \partial_x(huv) + \partial_y(hv^2 + \frac{1}{2}gh^2) & = & -gh\partial_y b \end{array}\right\} \quad \text{in } \overline{\Omega}_{\text{wet}} \tag{1.10}$$

$$h = u = v = 0 \qquad\qquad \text{in } \overline{\Omega}_{\text{dry}} \tag{1.11}$$

where h, u and v are the water depth and depth-averaged horizontal velocities and g is the gravitational constant. The left-hand-side of the equations is in divergence form and governs conservation of mass and momentum, and the right hand side is a non-conservative gravitational acceleration in case the bottom is sloped. The shallow water equations are widely used to model free surface flows such as rivers, lakes and oceans. Besides the many applications, the shallow water equations are a prototype of balance law whose source term is a non-conservative product of measures.

There is a large amount of literature on finite-volume (FV) and discontinuous Galerkin (DG) schemes for the shallow water equations, among them virtually all papers cited in the references [3, 4, 5, 6, 7, 8, 9, 10, 11, 12, 13, 14, 15, 16, 17, 18, 19, 20, 21, 22], as well as the references given in the review article [23].

In the present paper we would like to revisit the key issues of well-balancing, positivity, and continuous versus discontinuous discretization of the bottom topography. We also comment on unphysically

method	computed	derived	well-balanced	positive	non-reflecting
ad-hoc	b, h	w=b+h	no	no	no
SGM	b, w	h=w-b	yes	no	yes
HRM	h, w	b=w-h	yes	yes	no
BSGM	b & w	h=w-b	yes	yes	yes

Table 1: Cartoon of the history of well-balanced, positivity preserving schemes. ad-hoc: standard non-well-balanced scheme. SGM: surface-gradient method by Zhou et al. [25]. HRM: hydrostatic reconstruction method by Audusse et al. [26]. BSGM: bottom-surface-gradient method (present).

reflected waves due to non-monotone reconstructions of the bottom, which were discussed and partially removed by Buttinger et al. [24].

FV and DG schemes approximate the solution by piecewise polynomial functions, which are reconstructed and evolved in time. Note that there are three variables related to the vertical space dimension, only two of which are independent:

$$b(x, y), \quad w(x, y, t) \quad \text{and} \quad h(x, y, t) := w(x, y, t) - b(x, y). \tag{1.12}$$

This plays a role near the lake-at rest, which is often described as

$$u = v = 0, \quad h\partial_x w = 0, \quad h\partial_y w = 0 \tag{1.13}$$

(compare Definition 4.1 for a more complete statement).

Our point of view in the present manuscript is to distinguish the schemes by the choice of vertical variables which are reconstructed respectively derived, and which properties this implies. A cartoon of the history of first- and second-order accurate FV schemes is presented in Table 1. For example, an ad-hoc scheme with continuous piecewise linear bottom b and piecewise constant or linear h, and with $w := b + h$ will not preserve a flat water surface, and it will probably not be well-balanced.

The surface-gradient method (SGM) by Zhou et al. [25] reconstructs w instead of h, and hence is able to preserve the Lake-at-Rest. Unfortunately the water depth, which is now derived as $h = w - b$ may become negative near wet-dry fronts. This is cured in the hydrostatic reconstruction method (HRM) by Audusse et al. [26], who reconstruct and evolve w and h and derive the topography as $b = w - h$. As a consequence, the bottom becomes discontinuous at most interfaces and depends on time, even if the original bottom does not. Due to an ingenious discretization of the singular source term, the HRM is well-balanced and positivity preserving. Unfortunately, as observed by Buttinger et al., the HRM may produce unphysical wave reflections due to a non-monotone approximation of the bottom.

The bottom-surface-gradient method (BSGM) presented in this note unifies the SGM and the HRM. Starting from a continuous, piecewise linear or bi-linear bottom approximation, we start from a preliminary reconstruction of the water surface level w. As in the SGM, it may happen that this reconstruction of b and w produces negative water-heights $h = w - b$ in the interior of a cell. In this (and only this) case we move the front to one of the adjacent interfaces, and correct the reconstructions of both b and w simultaneously. The correction observes the minimum-maximum-preserving (MMP) principle in b and w. Note that the bottom is only discontinuous near a wet-dry front, or if the original topography happens to have a step. Only in these cases the source term is singular, and only here we compute the residuum with the subcell HRM [17]. The resulting scheme is well-balanced, positivity-preserving, and due to the MMP reconstruction it creates no unphysical reflections. It is simple and efficient, can be extended dimension by dimension to two-dimensional cartesian grids, and gives excellent computational results.

The paper is organized as follows: In Section 2, we introduce the bottom-surface gradient reconstruction. In Section 3 we define the finite volume update, including the hydrostatic reconstruction and the computation of the singular source terms. In Section 4 we establish the positivity and well-balancing properties in one space dimension. The two-dimensional extension is given in Section 5. In Section 6, we present numerical experiments which demonstrate second-order accuracy, well-balancing and positivity. We compute several one-dimensional Riemann problems and two-dimensional dambreak problems for which state-of-the art schemes may produce unphysical reflections. These demonstrate the quality of the BSGM.

2. Piecewise linear reconstruction

Let $\Omega \subset \mathbb{R}$ be a one-dimensional domain, and let $b : \Omega \to \mathbb{R}$ be the given topography. Discretize the domain as $\Omega = \bigcup_{i \in I} C_i$ with cells $C_i := (x_{i-\frac{1}{2}}, x_{i+\frac{1}{2}})$ and an index set $I \subset \mathbb{Z}$. For simplicity, we choose a uniform grid with $x_{i+\frac{1}{2}} - x_{i-\frac{1}{2}} = \Delta x$.

Let $h_i = h_i(t)$, $(hu)_i = (hu)_i(t)$ and $(hv)_i = (hv)_i(t)$ be the computed cell averages of the conserved variables, and let $w_i = w_i(t) = h_i(t) + b_i$ be the corresponding surface levels. First, we introduce wet and dry regions analogously to (1.4) and (1.5):

$$I_{wet}(t) := \{i \in I \mid h_i > 0\} \tag{2.1}$$

$$I_{dry}(t) := \{i \in I \mid h_i = 0\} \tag{2.2}$$

Then we distinguish between those cells which are adjacent to the wet-dry front, and those which are in the interior of the respective regions:

$$I_{wet}^{front}(t) := \{i \in I_{wet}(t) \mid \min(h_{i\pm 1}) = 0\}, \qquad I_{wet}^{int}(t) := I_{wet}(t) \setminus I_{wet}^{front}(t), \tag{2.3}$$

$$I_{dry}^{front}(t) := \{i \in I_{dry}(t) \mid \max(h_{i\pm 1}) > 0\}, \qquad I_{dry}^{int}(t) := I_{dry}(t) \setminus I_{dry}^{front}(t), \tag{2.4}$$

so $I_{wet}(t) = I_{wet}^{front}(t) \cup I_{wet}^{int}(t)$ and $I_{dry}(t) = I_{dry}^{front}(t) \cup I_{dry}^{int}(t)$.

In the following, we construct preliminary and corrected piecewise linear approximations of b, h, w and u.

2.1. Initial approximation of the bottom

Let b be the original bottom introduced in (1.1). The preliminary, piecewise linear reconstruction $b^{\#}$ is defined by

$$b^{\#}(x) := b^r_{i-\frac{1}{2}} + \frac{x - x_{i-\frac{1}{2}}}{\Delta x}(b^l_{i+\frac{1}{2}} - b^r_{i-\frac{1}{2}}) \quad \text{for } x \in C_i, \tag{2.5}$$

where $b^r_{i-\frac{1}{2}} := b(x_{i-\frac{1}{2}} + 0)$ and $b^l_{i+\frac{1}{2}} := b(x_{i+\frac{1}{2}} - 0)$. Note that $b^{\#}$ is continuous at $x_{i+\frac{1}{2}}$ if and only if b is continuous. Let $b_i := b^{\#}(x_i)$ be the value of $b^{\#}$ at the cell center, and let $\partial^{\#}_x b_i := (b^l_{i+\frac{1}{2}} - b^r_{i-\frac{1}{2}})/\Delta x$ be the local slope.

2.2. Preliminary reconstruction of the flow variables

Define the velocities by

$$(u_i, v_i) := \begin{cases} \left(\frac{(hu)_i}{h_i}, \frac{(hv)_i}{h_i}\right) & \text{if } h_i > \varepsilon, \\ (0, 0) & \text{otherwise,} \end{cases} \tag{2.6}$$

where ε is a small a-priori chosen positive number to avoid the division by very small numbers. In this paper, we choose $\varepsilon = 1.0 \times 10^{-10}$.

For any scalar quantity $q \in \{w, u, v\}$, we define a preliminary, discontinuous, piecewise linear reconstruction by

$$q^{\#}(x, t) := q_i(t) + (x - x_i)\, \partial^{\#}_x q_i(t) \quad \text{for } x \in C_i, \tag{2.7}$$

where $\partial^{\#}_x q_i$ is an approximate slope of q in the cell. If $i \in I^{int}_{dry}(t)$ we simply set

$$\partial^{\#}_x u_i = \partial^{\#}_x v_i = 0, \quad \partial^{\#}_x w_i = \partial^{\#}_x b_i. \tag{2.8}$$

Otherwise if $i \in I_{wet}(t) \cup I^{front}_{dry}(t)$, we compute the slope using a standard limiter function. We choose

$$\partial^{\#}_x q_i := \operatorname{minmod}\left(\theta \frac{q_i - q_{i-1}}{\Delta x}, \frac{q_{i+1} - q_{i-1}}{2\Delta x}, \theta \frac{q_{i+1} - q_i}{\Delta x}\right), \tag{2.9}$$

with minmod function

$$\operatorname{minmod}(a_1, a_2, \cdots, a_m) := \begin{cases} \max\limits_i a_i, & \text{if } \max\limits_i a_i < 0, \\ \min\limits_i a_i, & \text{if } \min\limits_i a_i > 0, \\ 0, & \text{otherwise.} \end{cases} \tag{2.10}$$

The parameter $\theta \in [1, 2]$ controls the numerical viscosity of the numerical scheme. We set $\theta := 1.3$. Finally, we define the preliminary height by

$$h^{\#}(x, t) := w^{\#}(x, t) - b^{\#}(x, t). \tag{2.11}$$

For future reference we also introduce the one-sided limits

$$q^l_{i+\frac{1}{2}}(t) := q^{\#}(x_{i+\frac{1}{2}} - 0, t), \tag{2.12}$$

$$q^r_{i+\frac{1}{2}}(t) := q^{\#}(x_{i+\frac{1}{2}} + 0, t) \tag{2.13}$$

for $q \in \{h, u, v, w\}$.

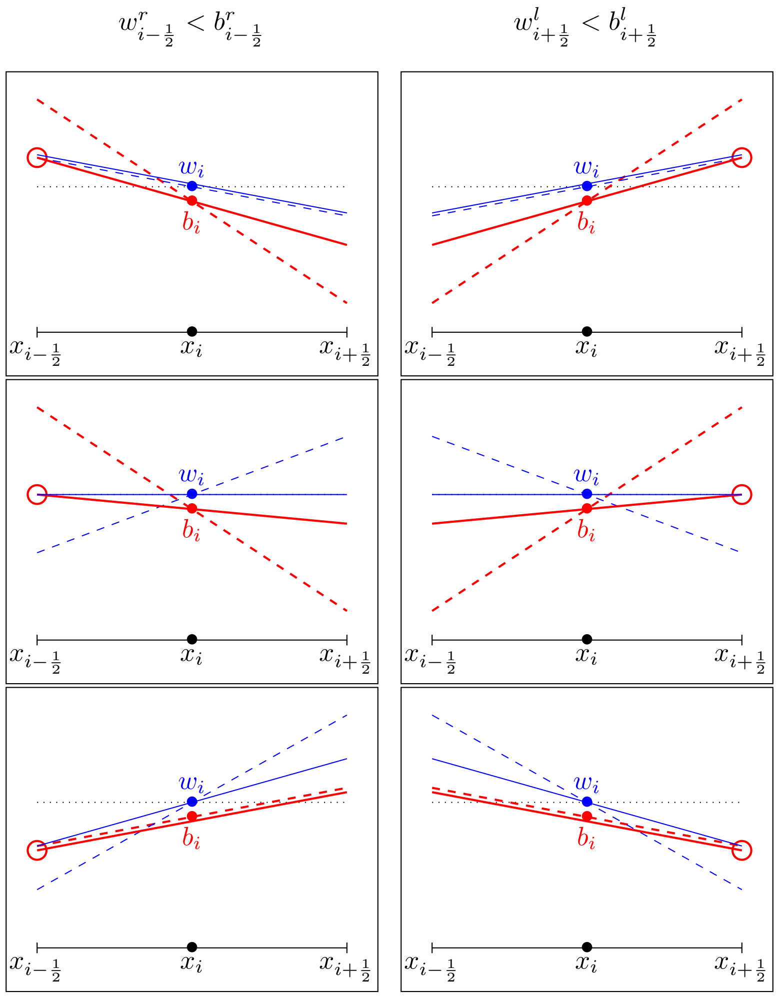

Figure 1: The BSGM reconstruction for a cell C_i which is wet-dry at time t. Left column: interface $(i-\frac{1}{2})$ is wet-dry at time t. Right column: interface $(i+\frac{1}{2})$ is wet-dry at time t. Preliminary reconstruction: red dashed lines: $b_i^{\#}(x,t)$; blue dashed lines: $w_i^{\#}(x,t)$. Corrected reconstruction: red lines: $b_i^{\#\#}(x,t)$; blue lines: $w_i^{\#\#}(x,t)$. Upper row: only $\partial_x^{\#} b$ is limited. Center row: both $\partial_x^{\#} b$ and $\partial_x^{\#} w$ are limited. Lower row: only $\partial_x^{\#} w$ is limited. The interface levels $z_{i-\frac{1}{2}+}$ and $z_{i+\frac{1}{2}-}$ are marked by red circles.

2.3. Corrected reconstruction

In this section we correct the piecewise linear reconstruction in wet-dry cells, which are identified by

$$I^{\#}_{wetdry}(t) = \left\{ i \in I | \min_{x \in C_i} h^{\#}(x,t) < 0 < \max_{x \in C_i} h^{\#}(x,t) \right\}. \tag{2.14}$$

Note that $I^{\#}_{wetdry}(t) \subset I_{wet}(t) \cup I^{front}_{dry}(t)$, since $h^{\#}$ vanishes identically in $I^{int}_{dry}(t)$. It would be interesting to see if $I^{\#}_{wetdry}(t) \subset I^{front}_{wet}(t) \cup I^{front}_{dry}(t)$, i.e. if wet-dry cells could also occur in the interior $I^{int}_{wet}(t)$ of wet regions.

Let $i \in I^{\#}_{wetdry}(t)$. Since the minimum of $h^{\#}(\cdot,t)$ lies at one of the endpoints $x_{i\pm 1/2}$, we distinguish two cases:

- If $w^r_{i-\frac{1}{2}}(t) < b^r_{i-\frac{1}{2}}(t)$, we call the left interface $(i-\frac{1}{2})$ a *wet-dry front at time* t and set

$$z_{i-\frac{1}{2}+}(t) := w_i(t) + \mathrm{minmod}(w^r_{i-\frac{1}{2}}(t) - w_i(t), b^r_{i-\frac{1}{2}}(t) - w_i(t)). \tag{2.15}$$

  For $q \in \{b, w\}$ we redefine the slopes by

$$\partial_x^{\#\#} q_i(t) := 2\frac{q_i(t) - z_{i-\frac{1}{2}+}(t)}{\Delta x}. \tag{2.16}$$

- If $w^l_{i+\frac{1}{2}}(t) < b^l_{i+\frac{1}{2}}(t)$, we call the right interface $(i+\frac{1}{2})$ a *wet-dry front at time* t and set

$$z_{i+\frac{1}{2}-}(t) := w_i(t) + \mathrm{minmod}(w^l_{i+\frac{1}{2}}(t) - w_i(t), b^l_{i+\frac{1}{2}}(t) - w_i(t)). \tag{2.17}$$

  For $q \in \{b, w\}$ we redefine the slopes by

$$\partial_x^{\#\#} q_i(t) = 2\frac{z_{i+\frac{1}{2}-}(t) - q_i(t)}{\Delta x}. \tag{2.18}$$

Once more, let $q \in \{b, w\}$. Given the modified slopes $\partial_x^{\#\#} q_i(t)$, the corrected reconstruction is

$$q_i^{\#\#}(x,t) := \begin{cases} q_i(t) + (x - x_i)\partial_x^{\#\#} q_i(t) & \text{if } i \in I^{\#}_{wetdry}(t), \\ q^{\#}(x,t) & \text{otherwise.} \end{cases} \tag{2.19}$$

The corrected reconstructions of h, u and v are given by

$$h^{\#\#}(x,t) := w^{\#\#}(x,t) - b^{\#\#}(x,t) \tag{2.20}$$

$$u^{\#\#}(x,t) := u^{\#}(x,t), \tag{2.21}$$

$$v^{\#\#}(x,t) := v^{\#}(x,t). \tag{2.22}$$

For $q \in \{b, h, u, v, w\}$, we denote the one-sided limits of the corrected reconstruction by

$$q_{i+\frac{1}{2}-}(t) := q^{\#\#}(x_{i+\frac{1}{2}} - 0, t), \tag{2.23}$$

$$q_{i+\frac{1}{2}+}(t) := q^{\#\#}(x_{i+\frac{1}{2}} + 0, t). \tag{2.24}$$

Please note the subtle difference with the notation for the edge values $q^{l/r}_{i\pm\frac{1}{2}}(t)$ of the preliminary reconstruction $q^{\#}(x,t)$, see (2.12), (2.13)).

Remark 2.1. (i) We call (2.19) - (2.21) the bottom-surface-gradient (BSGM) reconstruction.

(ii) Figure 1 shows the details of the BSGM correction for bottom and surface in a wet-dry cell.

2.4. Stability properties of the BSGM-reconstruction

The BSGM reconstruction satisfies the following monotonicity properties:

Theorem 2.2. *At the left interface of cell C_i,*

$$h_{i-\frac{1}{2}+} \geq 0 \qquad \textit{for all } i \in I, \tag{2.25}$$

$$\min(w_{i-1}, w_i) \leq w_{i-\frac{1}{2}+} \leq \max(w_{i-1}, w_i) \qquad \textit{for all } i \in I_{wet}(t) \cup I^{front}_{dry}(t) \tag{2.26}$$

$$\min(b^r_{i-\frac{1}{2}}, b_i) \leq b_{i-\frac{1}{2}+} \leq \max(b^r_{i-\frac{1}{2}}, b_i) \qquad \textit{for all } i \in I^{\#}_{wetdry}(t) \tag{2.27}$$

and analogously at the right interface,

$$h_{i+\frac{1}{2}-} \geq 0 \qquad \textit{for all } i \in I, \tag{2.28}$$

$$\min(w_i, w_{i+1}) \leq w_{i+\frac{1}{2}-} \leq \max(w_i, w_{i+1}) \qquad \textit{for all } i \in I_{wet}(t) \cup I_{dry}^{front}(t) \tag{2.29}$$

$$\min(b_i, b^l_{i+\frac{1}{2}}) \leq b_{i+\frac{1}{2}} - \leq \max(b_i, b^l_{i+\frac{1}{2}}) \qquad \textit{for all } i \in I^{\#}_{wetdry}(t). \tag{2.30}$$

Remark 2.3 (MMP property of the bottom reconstruction)*.* Theorem 2.2 lays the basis for the stability analysis of the BSGM scheme in Section 4. In particular, (2.27) and (2.30) mean that the corrected reconstruction of the bottom in wet-dry cells, $b^{\#\#}(x,t)$, is maximum-minimum-preserving (MMP). This is in contrast with previous HR schemes [26, 17], and our numerical experiments indicate that this helps to avoid unphysical reflected waves in the numerical solution.

Proof. By the monotonicity of the minmod function (2.10), we have that after the preliminary reconstruction

$$\min(w_{i-1}, w_i) \leq w^r_{i-\frac{1}{2}} \leq \max(w_{i-1}, w_i), \tag{2.31a}$$

$$\min(w_i, w_{i+1}) \leq w^l_{i+\frac{1}{2}} \leq \max(w_i, w_{i+1}). \tag{2.31b}$$

Thus the sufficient conditions for (2.26) and (2.29) are

$$\min(w^r_{i-\frac{1}{2}}, w_i) \leq w_{i-\frac{1}{2}+} \leq \max(w^r_{i-\frac{1}{2}}, w_i) \tag{2.32a}$$

$$\min(w_i, w^l_{i+\frac{1}{2}}) \leq w_{i+\frac{1}{2}-} \leq \max(w_i, w^l_{i+\frac{1}{2}}), \tag{2.32b}$$

By the linearity of both $w^{\#}_i(x)$ and $w^{\#\#}_i(x)$ in cell I_i, we know that (2.32a) and (2.32b) are equivalent. Similarly we get the equivalence between (2.27) and (2.30). These tell us that we only need to prove (2.32a,2.27) or (2.32b,2.30).

We next move to effect of corrected reconstruction step. Let $i \in I^{\#}_{wetdry}(t)$ in where the correction step is activated.

Without losing generality we first consider the case that the right interface $(i + \frac{1}{2})$ is a wet-dry front at time t, i.e. $w^l_{i+\frac{1}{2}} < b^l_{i+\frac{1}{2}}$. Notice that the reconstructed surface level and bottom at $x_{i+\frac{1}{2}}$ in cell I_i share the same value $w_{i+\frac{1}{2}-} = b_{i+\frac{1}{2}-} = z_{i+\frac{1}{2}-}$ with the new freedom $z_{i+\frac{1}{2}-}$ defined by (2.15). Thus (2.32b,2.30) are equivalent to the following inequalities

$$\min(w_i, w^l_{i+\frac{1}{2}}) \leq z_{i+\frac{1}{2}-} \leq \max(w_i, w^l_{i+\frac{1}{2}}), \quad \min(b_i, b^l_{i+\frac{1}{2}}) \leq z_{i+\frac{1}{2}-} \leq \max(b_i, b^l_{i+\frac{1}{2}}). \tag{2.33}$$

By the property of the minmod function (2.10), the value of $z_{i+\frac{1}{2}-}$ dependent on the three quantities $w^l_{i+\frac{1}{2}}$, $b^l_{i+\frac{1}{2}}$ and w_i by

$$z_{i+\frac{1}{2}-} = \begin{cases} w^l_{i+\frac{1}{2}}, & w_i \leq w^l_{i+\frac{1}{2}} < b^l_{i+\frac{1}{2}} \\ w_i, & w^l_{i+\frac{1}{2}} \leq w_i \leq b^l_{i+\frac{1}{2}} \\ b^l_{i+\frac{1}{2}}, & w^l_{i+\frac{1}{2}} < b^l_{i+\frac{1}{2}} \leq w_i \end{cases} \tag{2.34}$$

which means that $z_{i+\frac{1}{2}-}$ choose the value of w_i if $w^l_{i+\frac{1}{2}}$ and $b^l_{i+\frac{1}{2}}$ are located at different sides of w_i; otherwise choose the closer one in $w^l_{i+\frac{1}{2}}$ and $b^l_{i+\frac{1}{2}}$ from w_i (see also from the Figure 1). It is checked from above equation that the value of $z_{i+\frac{1}{2}-}$ satisfies the relation (2.33). Then (2.32b,2.30) and further (2.26, (2.29), 2.27) and (2.30) hold.

The positivity (2.25) and (2.28) comes from the fact $b_{i+\frac{1}{2}-} = w_{i+\frac{1}{2}-} = z_{i+\frac{1}{2}-}$ which deduces that $h_{i+\frac{1}{2}-} = 0$ and then $h_{i-\frac{1}{2}+} = 2h_i - h_{i+\frac{1}{2}-} = 2h_i$ for cell $i \in I^{\#}_{wetdry}(t)$.

If the left interface $(i+\frac{1}{2})$ is a wet-dry front at time t, i.e. $w^r_{i-\frac{1}{2}} < b^r_{i-\frac{1}{2}}$. Analogously we can prove (2.32a,2.27) then (2.26, (2.29), 2.27) and (2.30). The positivity (2.25) and (2.28) is that $h^r_{i-\frac{1}{2}} = 0$ and $h_{i+\frac{1}{2}-} = 2h_i$ for cell $i \in I^{\#}_{wetdry}(t)$.

This concludes the proof. □

3. Finite volume update in 1D

In this section we suppose that the corrected reconstructions $q^{\#\#}(x,t)$ are already constructed, and, in particular, the corrected one-sided limits $q_{i+\frac{1}{2}\pm}$ are given by (2.23) - (2.24).

We rewrite the one-dimensional shallow water equations as

$$\partial_t U + \partial_x F(U) = S(U,x). \tag{3.1}$$

with

$$U := \begin{pmatrix} h \\ hu \\ hv \end{pmatrix}, \quad F(U) := \begin{pmatrix} hu \\ hu^2 + \frac{1}{2}gh^2 \\ huv \end{pmatrix} \quad \text{and} \quad S(U,x) := -\begin{pmatrix} 0 \\ gh\partial_x b(x) \\ 0 \end{pmatrix}. \tag{3.2}$$

As in [17], we start with a semi-discrete method of lines for the cell averages $U_i(t)$,

$$\frac{d}{dt}U_i(t) = R_i(t) := -\frac{1}{\Delta x}\left(F_{i+\frac{1}{2}} - F_{i-\frac{1}{2}}\right) + S_{i-\frac{1}{2}+} + S_i + S_{i+\frac{1}{2}-} \tag{3.3}$$

Based on the reconstruction of the previous section, we compute the central source term as

$$S_i := \left(0, -g\,\frac{h_{i-\frac{1}{2}+} + h_{i+\frac{1}{2}-}}{2}\,\frac{b_{i+\frac{1}{2}-} - b_{i-\frac{1}{2}+}}{\Delta x}, 0\right)^T. \tag{3.4}$$

If $b_{i+\frac{1}{2}-} = b_{i+\frac{1}{2}+}$, then the singular source terms $S_{i+\frac{1}{2}\pm}$ vanish. If the bottom is discontinuous (either because of the initial data (2.5) or because of the BSGM correction (2.16) (2.18)), then we compute hydrostatic reconstruction values $b^\star_{i+\frac{1}{2}}, U^\star_{i+\frac{1}{2}\pm}$ as in [17, (2.15)-(2.16)]:

$$b^\star_{i+\frac{1}{2}} := \min(w_{i+\frac{1}{2}-}, w_{i+\frac{1}{2}+}, \max(b_{i+\frac{1}{2}-}, b_{i+\frac{1}{2}+})), \tag{3.5}$$

$$h^\star_{i+\frac{1}{2}-} := \min(w_{i+\frac{1}{2}-} - b^\star_{i+\frac{1}{2}}, h_{i+\frac{1}{2}-}), \tag{3.6}$$

$$h^\star_{i+\frac{1}{2}+} := \min(w_{i+\frac{1}{2}+} - b^\star_{i+\frac{1}{2}}, h_{i+\frac{1}{2}+}), \tag{3.7}$$

$$(hu)^\star_{i+\frac{1}{2}\pm} := h^\star_{i+\frac{1}{2}\pm}\, u_{i+\frac{1}{2}\pm}, \tag{3.8}$$

$$(hv)^\star_{i+\frac{1}{2}\pm} := h^\star_{i+\frac{1}{2}\pm}\, v_{i+\frac{1}{2}\pm}. \tag{3.9}$$

Note that this also defines the vectors $U^\star_{i+\frac{1}{2}\pm}$. Then we evaluate the singular source terms following [17, (2.17)-(2.18)]:

$$s_{i+\frac{1}{2}-} := -g \, \frac{h_{i+\frac{1}{2}-} + h^\star_{i+\frac{1}{2}-}}{2} \, \frac{b^\star_{i+\frac{1}{2}} - b_{i+\frac{1}{2}-}}{\Delta x}, \tag{3.10}$$

$$s_{i+\frac{1}{2}+} := -g \, \frac{h_{i+\frac{1}{2}+} + h^\star_{i+\frac{1}{2}-}}{2} \, \frac{b_{i+\frac{1}{2}+} - b^\star_{i+\frac{1}{2}}}{\Delta x}. \tag{3.11}$$

and set

$$S_{i+\frac{1}{2}\pm} := (0, s_{i+\frac{1}{2}\pm}, 0)^T. \tag{3.12}$$

Finally, we compute the numerical flux evaluating the Harten-Lax-Van Leer Riemann solver at the hydrostatic values,

$$F_{i+\frac{1}{2}} := \mathcal{F}_{\mathrm{HLL}}(U^*_{i+\frac{1}{2}-}, U^*_{i+\frac{1}{2}+}). \tag{3.13}$$

Plugging (3.4), (3.12) and (3.13) into (4.19) determines the semi-discrete update.

Remark 3.1. In all but a few exceptional cases, the bottom will be continuous across the cell interface $b_{i+\frac{1}{2}-} = b_{i+\frac{1}{2}+}$. In this case the singular source terms vanish, and (3.12), (3.13) may be replaced by

$$S_{i+\frac{1}{2}\pm} = 0, \quad F_{i+\frac{1}{2}} := \mathcal{F}_{\mathrm{HLL}}(U_{i+\frac{1}{2}-}, U_{i+\frac{1}{2}+}). \tag{3.14}$$

To enhance efficiency of the code, we recommend to use a continuous bottom together with (3.14) whenever possible.

The fully-discrete update is computed by applying Heun's second-order accurate SSP Runge-Kutta method [27, 28] to the semi-discrete system (4.19).

4. Positivity and well-balancing in 1D

To capture the wet-dry front more precisely, we re-define

Definition 4.1 (lake-at-rest)**.** The solution of the shallow water equations is at rest (or satisfies the *Lake-at-Rest condition*) if for all $t \in [0, T]$

$$u(x,t) = v(x,t) = 0 \quad \text{for } x \in \Omega \tag{4.1}$$

$$\partial_x w(x,t) = 0 \quad \text{for } x \in \Omega_{wet}(t), \tag{4.2}$$

$$\lim_{\substack{x \to x_F \\ x \in \Omega_{wet}(t)}} w(x,t) \le \max\Big(\lim_{\substack{x \to x_F \\ x \in \Omega_{dry}(t)}} b(x), \lim_{\substack{x \to x_F \\ x \in \Omega_{wet}(t)}} b(x) \Big) \quad \text{for } x_F \in \Gamma(t). \tag{4.3}$$

Condition (4.3) means that at the wet-dry front, the dry bottom should be at least as high as the adjacent water surface, and keeps the water from flowing out of the wet region.

Now we define a discrete lake-at-rest state:

Definition 4.2 (discrete lake-at-rest)**.** We say that an approximate solution U_i^n satisfies the *discrete lake-at-rest condition* if the velocity vanishes everywhere,

$$u_i = v_i = 0 \quad \text{for all } i \in I, \tag{4.4}$$

the water surface level is constant in the interior of the wet region,

$$w_i = w_j \quad \text{for } i, j \in I_{wet}(t) \text{ and } |i-j| = 1 \tag{4.5}$$

and at the wet side of the front

$$w_i \leq b_j, \quad \text{for } i \in I_{wet}^{front}(t) \text{ and } j \in \{i \pm 1\} \cap I_{dry}(t). \tag{4.6}$$

Theorem 4.3. *Under the assumption that*

$$\frac{\Delta t}{\Delta x} \max(|u^n_{i+\frac{1}{2}\pm}| + \sqrt{g h^n_{i+\frac{1}{2}\pm}}) \leq \frac{1}{2}, \tag{4.7}$$

the scheme is positivity preserving, i.e. $h_i^{n+1} \geq 0$.

Proof. By (2.25) and (2.28), we have the positivity of the reconstructed water height $h_{i+\frac{1}{2}\pm} \geq 0$ at every cell interface. The subcell hydrostatic reconstruction (3.5) gives

$$0 \leq h^\star_{i-\frac{1}{2}+} \leq h_{i-\frac{1}{2}+}, \;\; 0 \leq h^\star_{i+\frac{1}{2}-} \leq h_{i+\frac{1}{2}-}. \tag{4.8}$$

Therefore

$$h_i = \frac{h_{i-\frac{1}{2}+} + h_{i+\frac{1}{2}-}}{2} \geq \frac{h^\star_{i-\frac{1}{2}+} + h^\star_{i+\frac{1}{2}-}}{2}. \tag{4.9}$$

Thus we have the lower bound estimation of the one step forward Euler method

$$\begin{aligned} h_i + \Delta t \, R_i^{(h)} &= h_i - \frac{\Delta t}{\Delta x}\left(F^{(1)}_{i+\frac{1}{2}} - \mathbf{F}^{(1)}_{i-\frac{1}{2}}\right) \\ &\geq \frac{1}{2}\left(h^\star_{i-\frac{1}{2}+} + \frac{2\Delta t}{\Delta x}\mathcal{F}^{(1)}_{\text{HLL}}(U^\star_{i-\frac{1}{2}-}, U^\star_{i-\frac{1}{2}+})\right) + \frac{1}{2}\left(h^\star_{i+\frac{1}{2}-} - \frac{2\Delta t}{\Delta x}\mathcal{F}^{(1)}_{\text{HLL}}(U^\star_{i+\frac{1}{2}-}, U^\star_{i+\frac{1}{2}+})\right) \\ &\geq 0, \end{aligned} \tag{4.10}$$

where we have used the positivity property of the HLL flux [29, 30, 16] and the CFL condition (4.7). Since Heun's Runge-Kutta method is a strong-stability preserving (see e.g. [27, 28]), the final update is non-negative.

This concludes the proof. □

Theorem 4.4 (well-balancing for the 1D lake-at-rest)**.** *If the data at time $t = t^n$ satisfy the discrete lake-at-rest condition, then $R_i(t^n) = 0$ for all cells, so the scheme is well-balanced.*

Proof. Suppose the data at time $t = t^n$ satisfy the discrete Lake-at-Rest conditions accordin to Definition 4.2. It follows by inspection that

$$u_{i\pm\frac{1}{2}-} = u_{i\pm\frac{1}{2}+} = v_{i\pm\frac{1}{2}-} = v_{i\pm\frac{1}{2}+} = 0 \qquad \text{for all } i \in I \tag{4.11}$$

$$h^\star_{i\pm\frac{1}{2}-} = h^\star_{i\pm\frac{1}{2}+} =: h^\star_{i\pm\frac{1}{2}} \qquad \text{for all } i \in I \tag{4.12}$$

$$w^\star_{i-\frac{1}{2}} = w_{i-\frac{1}{2}+} = w_{i+\frac{1}{2}-} = w^\star_{i+\frac{1}{2}} \qquad \text{for all } i \in I_{wet}(t). \tag{4.13}$$

In particular, if $i \in I_{dry}(t)$, $h^\star_{i\pm\frac{1}{2}} = 0$. Then $R_i = 0$. For $i \in I_{wet}(t)$,

$$U^\star_{i\pm\frac{1}{2}-} = U^\star_{i\pm\frac{1}{2}+} =: U^\star_{i\pm\frac{1}{2}} = (h^\star_{i\pm\frac{1}{2}}, 0, 0)^\top \tag{4.14}$$

$$F_{i\pm\frac{1}{2}} = F(U^\star_{i\pm\frac{1}{2}}) = \left(0, \frac{g}{2}(h^\star_{i\pm\frac{1}{2}})^2, 0\right)^\top. \tag{4.15}$$

Note that the first components of all residual terms vanish,

$$R_i^{(1)} = R^{(1)}_{i-\frac{1}{2}+} = R^{(1)}_{i+\frac{1}{2}-} = 0.$$

Using (4.13) we can rewrite the second components of the source terms as

$$\begin{aligned}
S_i^{(2)} &= -g\,\frac{h_{i-\frac{1}{2}+} + h_{i+\frac{1}{2}-}}{2}\,\frac{(w_{i+\frac{1}{2}-} - h_{i+\frac{1}{2}-}) - (w_{i-\frac{1}{2}+} - h_{i-\frac{1}{2}+})}{\Delta x} \\
&= \frac{g}{2\Delta x}\left(\left(h_{i+\frac{1}{2}-}\right)^2 - \left(h_{i-\frac{1}{2}+}\right)^2\right) \\
&= \frac{1}{\Delta x}\left(F^{(2)}(U_{i+\frac{1}{2}-}) - F^{(2)}(U_{i-\frac{1}{2}}+)\right),
\end{aligned} \tag{4.16}$$

Similarly,

$$S^{(2)}_{i-\frac{1}{2}+} = \frac{1}{\Delta x}\left(F^{(2)}(U_{i-\frac{1}{2}+}) - F^{(2)}(U^\star_{i-\frac{1}{2}+})\right), \tag{4.17}$$

$$S^{(2)}_{i+\frac{1}{2}-} = \frac{1}{\Delta x}\left(F^{(2)}(U^\star_{i+\frac{1}{2}}) - F^{(2)}(U_{i+\frac{1}{2}-})\right). \tag{4.18}$$

Using (4.16) - (4.18) in (4.19) gives

$$\begin{aligned}
R_i &= -\frac{1}{\Delta x}\left(F_{i+\frac{1}{2}} - F_{i-\frac{1}{2}}\right) + S_{i-\frac{1}{2}+} + S_i + S_{i+\frac{1}{2}-} \\
&= \frac{g}{2\Delta x}\Big(-F(U^\star_{i+\frac{1}{2}}) + F(U^\star_{i-\frac{1}{2}}) + F(U_{i-\frac{1}{2}+}) - F(U^\star_{i-\frac{1}{2}}) \\
&\qquad + F(U_{i+\frac{1}{2}-}) - F(U_{i-\frac{1}{2}}+) + F(U^\star_{i+\frac{1}{2}}) - F(U_{i+\frac{1}{2}-})\Big) \\
&= 0.
\end{aligned} \tag{4.19}$$

This concludes the proof. □

5. Finite volume scheme in 2D

We extend the 1D finite volume scheme dimension by dimension to the 2D case. In particular, the 1D preliminary and modified reconstructions of Section 2 are carried over analogously to the y-direction. This yields a second-order accurate, positivity-preserving and well-balanced 2D solver.

6. Numerical experiments

In Example 6.1 we demonstrate second order accuracy for a smooth, two-dimensional solution. Example 6.2 shows well-balancing for a two-dimensional lake-at-rest solution and illustrates the activation of the BSGM correction at the wet-dry front. Section 6.3 shows various instances in 1D and 2D where unphysical wave-reflections due to non-monotonicty of the bottom reconstruction occur for previous second-order HR schemes. This is cured by the BSGM. The appendix provides details how we compute the reference for discontinuous bottom. In all examples, we use the gravitational constant $g = 9.812$.

6.1. Accuracy

We test the accuracy for a smooth, very thin water film in the domain $[0,1] \times [0,1]$ with periodic boundary conditions. The bottom topography and initial values are

$$\begin{aligned} b(x,y) &= \tfrac{1}{2}(\sin^2(\pi x) + \cos^2(\pi y)), \\ h(x,y,0) &= \tfrac{1}{2}\left(e^{\cos(2\pi x)} + e^{\sin(2\pi y)}\right) - e^{-1} + 0.00001, \\ u(x,y,0) &= \sin(\cos(2\pi x)), \quad v(x,y,0) = \cos(\sin(2\pi y)). \end{aligned} \tag{6.1}$$

Note that the minimal water height is 10^{-5}. We run the solution until final time $t = 0.04$, where it is still smooth. The reference solution is computed on 800×800 cells. The L^1-errors at final time are displayed in Table 2 and show second-order accuracy.

# cells	h error	EOC	hu error	EOC	hv error	EOC
50×50	1.67e-3	-	4.06e-3	-	3.96e-3	-
100×100	4.26e-4	1.97	9.73e-4	2.06	9.43e-4	2.07
200×200	1.02e-4	2.05	2.27e-4	2.09	2.20e-4	2.10
400×400	2.54e-5	2.01	4.51e-5	2.33	4.55e-5	2.27

Table 2: L^1-errors and experimental orders of convergence for Example 6.1.

6.2. Well-balancing and positivity

Here we test the BSGM scheme for a two-dimensional lake-at-rest, which includes dry areas. The domain is $[0,4] \times [0,2]$. The bottom topography is given by

$$b(x,y) = \begin{cases} 0.8e^{-r}, & r := 2(x-2)^2 + 4(y-1)^2 < \log\left(\frac{8}{5}\right), \\ 1 - 0.8e^{r}, & \text{otherwise.} \end{cases} \tag{6.2}$$

and the initial data are

$$u(x,y,t=0) = v(x,y,t=0) = 0, \quad h(x,t=0) = \begin{cases} \max(0.45 - b(x,y), 0), & r < \log(\frac{8}{5}), \\ \max(0.3 - b(x,y), 0), & \text{otherwise.} \end{cases} \tag{6.3}$$

The simulation is done on 200×100 uniform cells until final time $t = 0.15$. The steady states are preserved up to machine error. In Figure 3 we mark those cells where the corrected reconstruction step developed in Section 2.3 is applied. The dry area is located between the elliptical fronts. In the right figure we see that the correction is applied both at the wet side and at the dry side of the wet-dry front.

6.3. Bottom reflections

In this section we show examples the ABBKP and the BHNW schemes may cause non-physical reflections. We begin with a number of one-dimensional Riemann problems in Section 6.3.1, and conclude with two-dimensional dam break problems in Section 6.3.2.

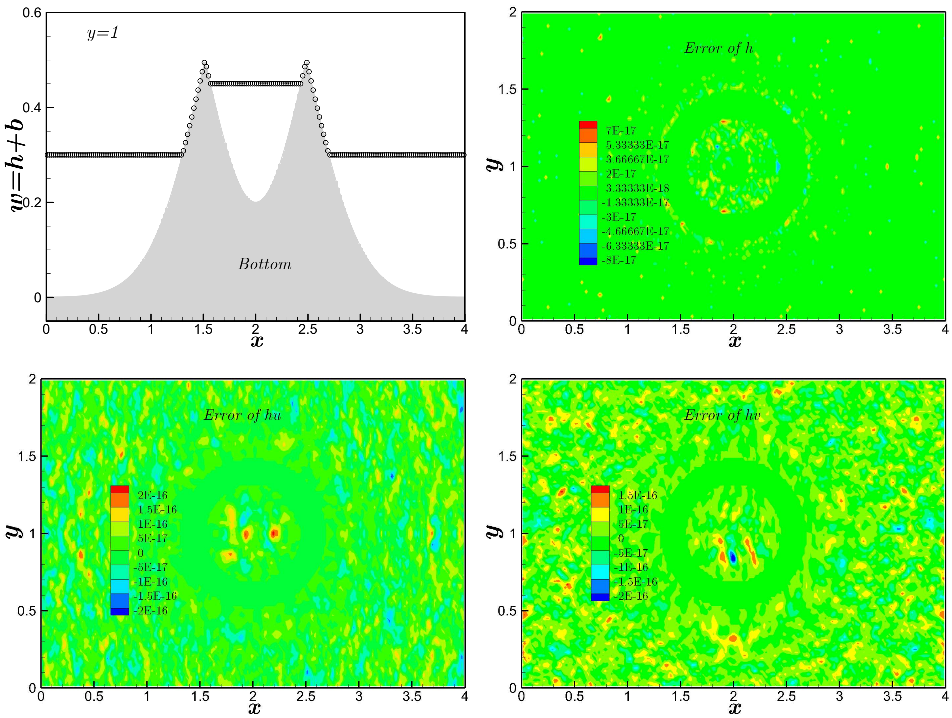

Figure 2: Two-dimensional well balanced test. 1-D slice (along y = 1) of the simulated result, and numerical errors of h, hu and hv. The simulation are done on 200×100 meshes.

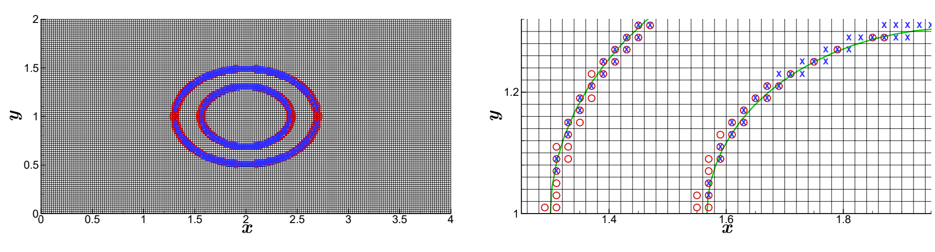

Figure 3: Two-dimensional well balanced test. Indicator where corrected reconstruction step is applied in x- direction (red circles) and y-direction (blue crosses), see Section 2.3. Full 200×100 grid (left) and detail (right).

6.3.1. One-dimensional Riemann problems

We have tested the three schemes on seven Riemann problems [24, 31, 32, 3] with $x \in [-1, 1]$ and with data (h_L, u_L, b_L) respectively (h_R, u_R, b_R) given in Table 3. All simulations are done until $t = 0.1$ on 1000 uniform cells. Since the bottom is discontinuous, we compute the reference solution by a careful limit process based on the recent analysis in [32, 33] which we detail in Appendix A. In the right columns of Table 3 we note whether the schemes produce unphysical reflections.

RP	h_L	h_R	u_L	u_R	b_L	b_R	ABBKP	BHNW	BSGM
1	4.0	0.50537954	0.1	0.0	0.0	1.5	ok	ok	ok
2	1.5	0.16664757	2.0	0.0	0.0	2.0	ok	ok	ok
3	0.3	0.4	2.0	2.2	1.1	1.0	ok	ok	ok
4	1.0	0.8	2.0	4.0	1.1	1.0	ok	ok	ok
5	0.75	1.0	0.0	0.0	1.0	0.0	REFL	REFL	ok
6	0.1	0.05	0.1	0.4	0.1	0.0	REFL	ok	ok
7	1.0	1.0	2.0	4.0	1.0	0.0	REFL	ok	ok

Table 3: Riemann problems. The initial left and right states with bottom jumps. ABBKP creates reflections in RP 5, 6, 7, and BHNW in RP 5.

In Figure 4 we display solutions of Riemann problems 4 and 5. The initial data of Riemann problem 4 are fully wet. Therefore, the corrected reconstructions of the BHNW and BSGM scheme are not activated, and all three solutions coincide.

On the other hand for the Riemann problem 5, the ABBKP and BHNW solutions exhibit a non-physical reflection originating at the origin, which is a partially wet point. To understand reflection, we show the bottom reconstructions of the three schemes in Figure 5.

6.3.2. Dam break over wet terrain

To highlight the issue of non-physical reflections, we consider two dam break problems over two-dimensional, discontinuous terrain. The domain is $(0, 300) \times (0, 200)$, the dam of height $b(x, y) = 20$ is located at $(85, 95) \times (0, 95)$ and $(85, 95) \times (170, 200)$, and in the remaining region, we initialize bottom and water depth by

$$(b(x,y), h(x,y,t=0)) = \begin{cases} (10, 7.5) & x < 90, \\ (0, 10) & x > 90. \end{cases} \tag{6.4}$$

The initial velocity is set to zero. We impose an outflow boundary condition at $y = 200$, and reflective boundary conditions at all other boundaries.

After the dam breaks, a shock wave propagates to the right, a rarefaction to the left, and a stationary shock is formed at the step. At later times, these waves interact with waves which are diffracted from the corners of the wall. In Figure 6, the numerical results for ABBKP, BHNW and BSGM on 600×400 cells are displayed at times $t = 3$, $t = 6$ and $t = 9$. The reference solution is

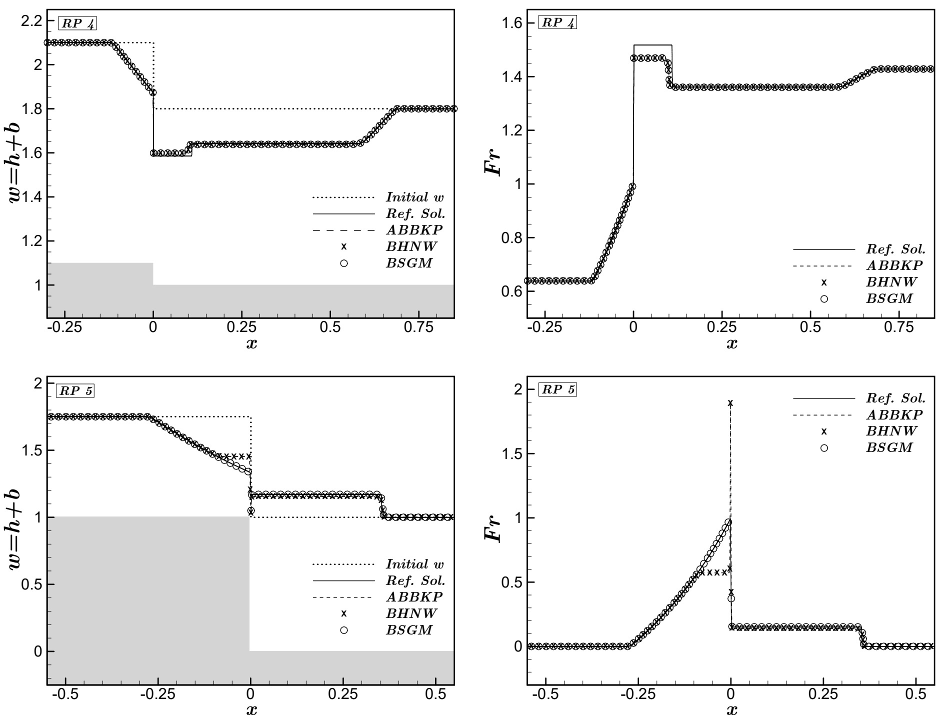

Figure 4: Riemann Problems 4 (top row) and 5 (bottom row). Comparison of schemes ABBKP, BHNW and BSGM. The three methods produce very close results and capture the wave patterns for Riemann problem 4. The ABBKP and the BHNW produce the same results and nonphysical reflection for Riemann Problem 5. The nonphysical refection is cured by the BSGM.

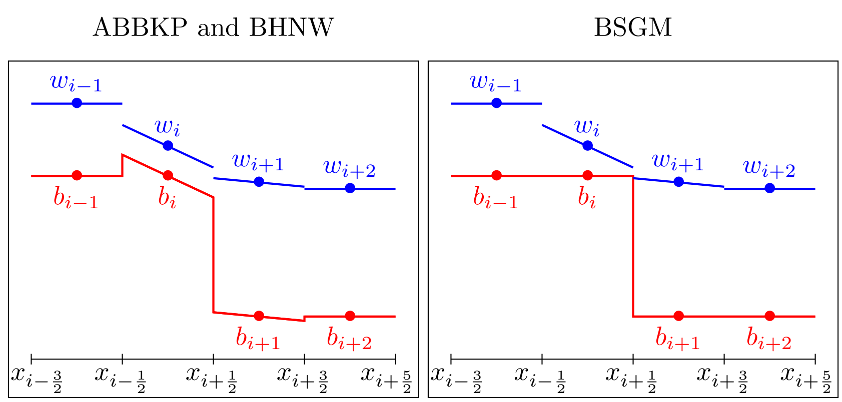

Figure 5: Reconstruction for Riemann problem 5. The ABBKP and the BHNW create unphysical local extrema in the bottom. The BSGM gives a MMP bottom reconstruction.

computed on 2400×1600 cells, with an additional layer of 8 cells where the bottom is smoothed. We plot 60 contours of the water surface, as well as two cross-sections along $y = 132.5$ and $y = 167.2$. Similarly to RP 5 in Figure 4, the ABBKP and the BHNW produce non-physical backward waves to the left of the step. Upon interacting with the waves diffracted from the corners of the wall, the schemes cannot recover the wave structure in the center and to the left of the dam break. Clearly, the result by BSGM is converging to the reference solution.

6.3.3. Dam break over dry terrain

Here we compute a dam break over dry terrain. The only difference to (6.4) is that $h(x, y, t = 0) = 0$ for $x > 90$. The numerical results are shown in Figure 7. Once more, the ABBKP produces a non-physical reflection. For this problem, both the BHNW and the BSGM schemes are reflection-free. While all three schemes preserve the positivity near the wet-dry front travelling to the right, the front position of the ABBKP scheme seems to be slightly lagging behind.

7. Conclusion

In this paper, we have revisited the key issues of well-balancing, positivity, and continuous versus discontinuous discretization of the bottom topography. The new bottom-surface-gradient reconstruction produces a bottom which is almost everywhere continuous, except at large physical discontinuities of the topography and at wet-dry fronts. In such situations, we reconstruct bottom and surface in one sweep which is maximum-minimum-preserving for both b and $w = h + b$. If bottom discontinuities remain, we apply the subcell hydrostatic reconstruction method to obain a well-balanced, positivity preserving and second-order-accurate scheme. Numerical experiments in one and two space dimension give excellent results. In particular, they demonstrate that the BSGM scheme does not produce unphysical reflections near bottom steps.

8. Acknowledgement

This work was supported in part by the National Science Foundation of China (11371023) and by the Deutsche Forschungsgemeinschaft under DFG grant 320021702/GRK2326.

Appendix A. Reference solution for discontinuous topography

When the bottom is continuous, we compute the reference solution by the first order subcell hydrostatic reconstruction scheme [17] on sufficiently refined grids. For discontinuous bottom the solution of the Riemann problem can be non-unique (see e.g. [32, 31] and the references therein). A key difficulty is the possible coincidence of stationary waves, which is called resonance. Aleksyuk and Belikov [33] single out a unique resonant solution by demanding that the discharge hu at $x = 0$ should depend continuously on the initial conditions. They construct this solution by approximating the bottom with a sequence of monotone functions.

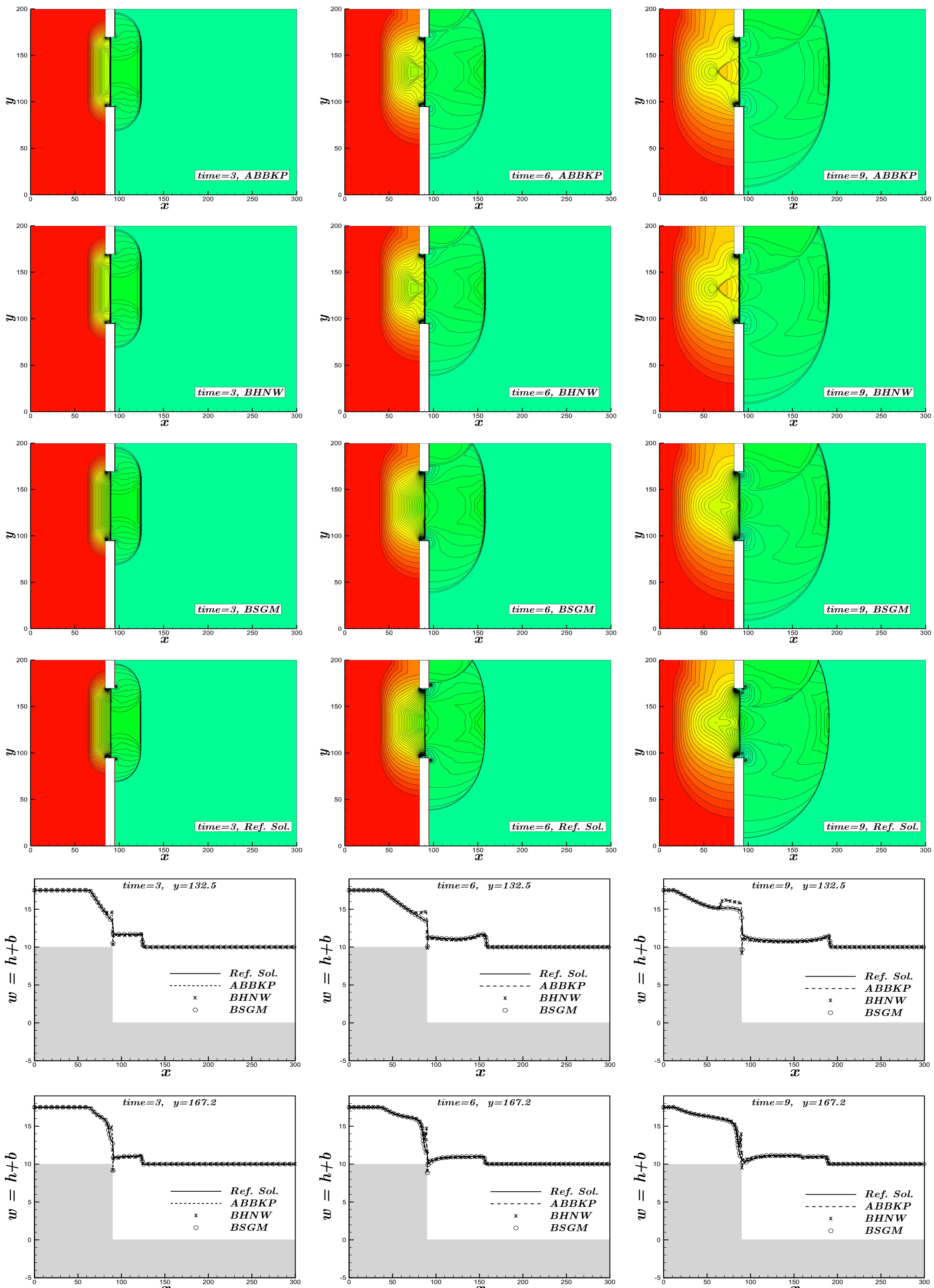

Figure 6: Water surface levels for the two-dimensional dam break problem over wet terrain. Top to bottom: ABBKP, BHNW, BSGM, reference solutions and cross sections at $y = 132.5$ and $y = 167.2$. Note the non-physical reflections to the left of the step.

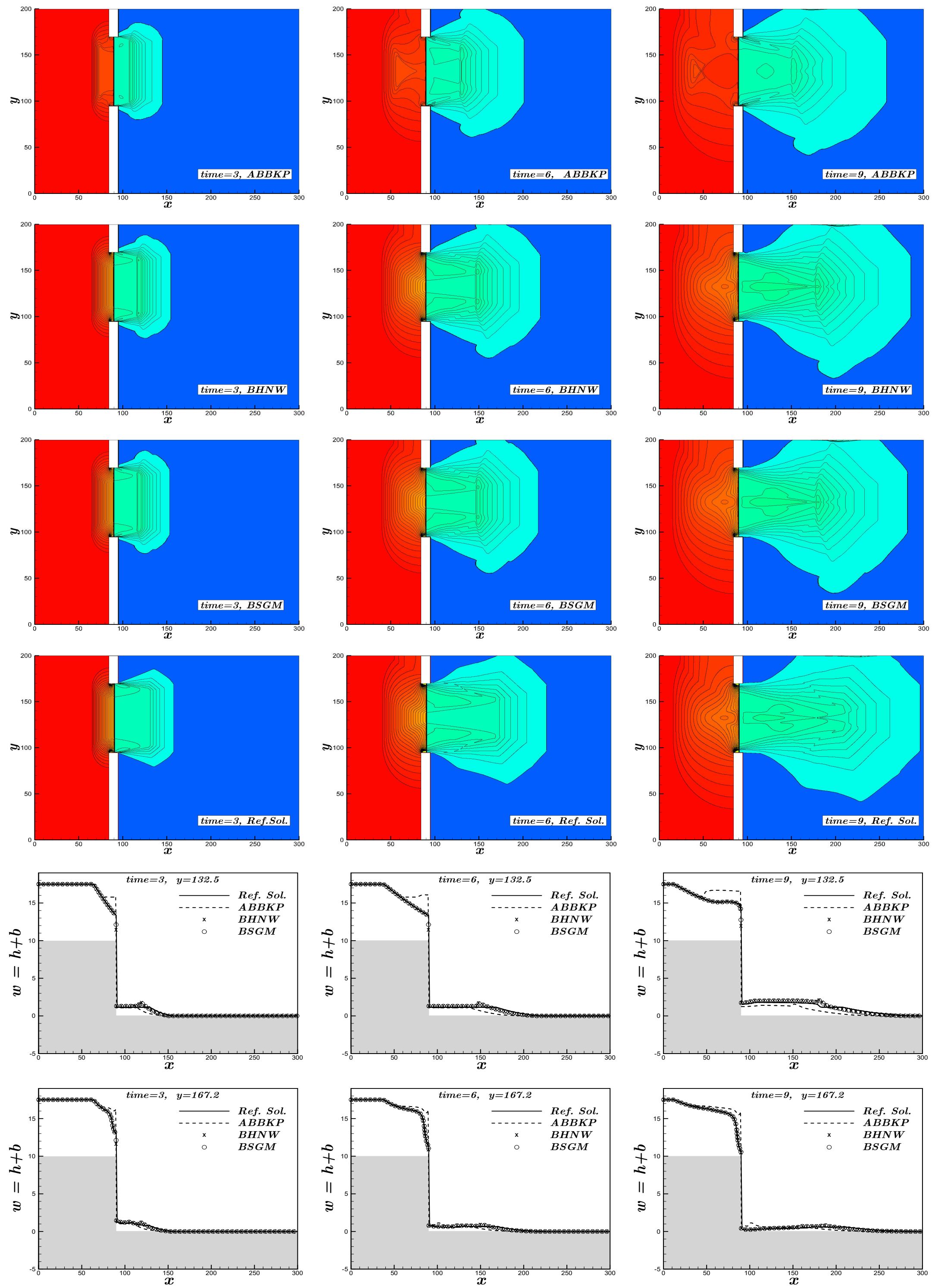

Figure 7: Analagous to Figure 6, but with dry bottom to the right of the step.

We follow this approach and approximate the topography linearly in a transition layer $(-\delta, \delta)$. Then we pass δ to zero numerically. At the same time, we increase the number of grid points in the transition layer. We denote the approximate solution for fixed $\delta > 0$ by U_δ and check numerically that

$$\|U_\delta\|_{L^\infty([-\delta,\delta])} \tag{A.1}$$

is uniformly bounded with respect to δ. This is evidence that the reference solution

$$U_{\text{ref}} := \lim_{\delta \to 0} U_\delta \tag{A.2}$$

is absolutely continuous with respect to Lebesgue measure. As a consequence, we do not display U_δ in the transition layer, which has Lebuesgue measure zero in the limit. Finally, we control that the discharge $(hu)_{\text{ref}}$ is continuous at $x = 0$.

References

[1] Saint-Venant, Théorie du mouvement non-permanent des eaux avec application aux crues des rivières et à l'introduction des mares dans leur lit, Comptes Rendus Hebdomadaires Des Séances De l'Académie Des Sciences 73 (1871) 147–154.

[2] J.-F. Gerbeau, B. Perthame, Derivation of viscous Saint-Venant system for laminar shallow water; numerical validation 1 (1) (2001) 89–102.

[3] J. Murillo, P. Garca-Navarro, Weak solutions for partial differential equations with source terms: Application to the shallow water equations, Journal of Computational Physics 229 (11) (2010) 4327–4368.

[4] M. Castro, J. M. Gallardo, C. Parés, High order finite volume schemes based on reconstruction of states for solving hyperbolic systems with nonconservative products. applications to shallow-water systems, Mathematics of Computation 75 (255) (2006) 1103–1134.

[5] J. M. Greenberg, A. Y. Leroux, A well-balanced scheme for the numerical processing of source terms in hyperbolic equations, SIAM Journal on Numerical Analysis 33 (1) (1996) 1–16.

[6] Z. Horváth, J. Waser, R. A. P. Perdigão, A. Konev, G. Blöschl, A two-dimensional numerical scheme of dry/wet fronts for the Saint-Venant system of shallow water equations, Internat. J. Numer. Methods Fluids 77 (3) (2015) 159–182.

[7] S. Jin, A steady-state capturing method for hyperbolic systems with geometrical source terms, Mathematical Modelling and Numerical Analysis 35 (4) (2001) 631–645.

[8] A. Kurganov, G. Petrova, A second-order well-balanced positivity preserving central-upwind scheme for the Saint-Venant system, Communications in Mathematical Sciences 5 (1) (2007) 133–160.

[9] D. S. Bale, R. J. Leveque, S. Mitran, J. A. Rossmanith, A wave propagation method for conservation laws and balance laws with spatially varying flux functions, SIAM J. Sci. Comput. 24 (3) (2002) 955–978.

[10] X. Liu, J. Albright, Y. Epshteyn, A. Kurganov, Well-balanced positivity preserving central-upwind scheme with a novel wet/dry reconstruction on triangular grids for the saint-venant system, Journal of Computational Physics 374 (2018) 213–236.

[11] Q. Liang, F. Marche, Numerical resolution of well-balanced shallow water equations with complex source terms, Advances in Water Resources 32 (6) (2009) 873–884.

[12] S. Noelle, Y. Xing, C.-W. Shu, High-order well-balanced finite volume WENO schemes for shallow water equation with moving water, Journal of Computational Physics 226 (1) (2007) 29–58.

[13] J. M. Gallardo, M. Castro, C. Parés, J. M. González-Vida, On a well-balanced high-order finite volume scheme for the shallow water equations with bottom topography and dry areas, Journal of Computational Physics 227 (1) (2007) 574–601.

[14] Y. Xing, X. Zhang, C.-W. Shu, Positivity-preserving high order well-balanced discontinuous Galerkin methods for the shallow water equations☆☆☆, Advances in Water Resources 33 (12) (2010) 1476–1493.

[15] Y. Xing, X. Zhang, Positivity-preserving well-balanced discontinuous Galerkin methods for the shallow water equations on unstructured triangular meshes, Journal of Scientific Computing 57 (2013) 19C41.

[16] A. Bollermann, G. Chen, A. Kurganov, S. Noelle, A well-balanced reconstruction of wet/dry fronts for the shallow water equations, Journal of Scientific Computing 56 (2) (2013) 267–290.

[17] G. Chen, S. Noelle, A new hydrostatic reconstruction scheme based on subcell reconstructions, SIAM Journal on Numerical Analysis 55 (2) (2017) 758–784.

[18] C. Berthon, A. Duran, F. Foucher, K. Saleh, J. D. D. Zabsonre, Improvement of the hydrostatic reconstruction scheme to get fully discrete entropy inequalities, Journal of Scientific Computing 80 (2) (2019) 924–956.

[19] M. Lukacova-Medvidova, S. Noelle, M. Kraft, Well-balanced finite volume evolution Galerkin methods for the shallow water equations, Journal of Computational Physics 221 (1) (2007) 122–147.

[20] C. Klingenberg, A. Kurganov, M. Zenk, Moving-water equilibria preserving HLL-type schemes for the shallow water equations, Communications in Mathematical Research 36 (3) (2020) 247–271.

[21] J. Dong, D. F. Li, A reliable second-order hydrostatic reconstruction for shallow water flows with the friction term and the bed source term, Journal of Computational and Applied Mathematics 376 (2020) 112871.

[22] J. Dong, D. F. Li, Exactly well-balanced positivity preserving nonstaggered central scheme for open-channel flows, Internat. J. Numer. Methods Fluids 93 (1) (2021) 273–292.

[23] A. Kurganov, Finite-volume schemes for shallow-water equations, Acta Numer. 27 (2018) 289–351.

[24] A. Buttinger-Kreuzhuber, Z. Horváth, S. Noelle, G. Blöschl, J. Waser, A fast second-order shallow water scheme on two-dimensional structured grids over abrupt topography, Advances in Water Resources 127 (2019) 89–108.

[25] J. G. Zhou, D. M. Causon, C. G. Mingham, D. M. Ingram, The surface gradient method for the treatment of source terms in the shallow-water equations, Journal of Computational Physics 168 (1) (2001) 1–25.

[26] E. Audusse, F. Bouchut, M.-O. Bristeau, R. Klein, B. Perthame, A fast and stable well-balanced scheme with hydrostatic reconstruction for shallow water flows, SIAM Journal on Scientific Computing 25 (6) (2004) 2050–2065.

[27] C.-W. Shu, TVB uniformly high-order schemes for conservation laws, Mathematics of Computation 49 (179) (1987) 105–121.

[28] G. Sigal, D. Ketcheson, C.-W. Shu, Strong stability preserving Runge-Kutta and multistep time discretizations, World Scientific, Singapore, 2011.

[29] B. Einfeldt, C. D. Munz, P. L. Roe, B. Sjögreen, On Godunov-type methods near low densities, Journal of Computational Physics 92 (2) (1991) 273–295.

[30] F. Bouchut, Nonlinear stability of finite volume methods for hyperbolic conservation laws and well-balanced schemes for sources, Springer Science & Business Media, 2004.

[31] E. Han, G. Warnecke, Exact Riemann solutions to shallow water equations, Quarterly of Applied Mathematics 72 (3) (2014) 407–453.

[32] P. G. LeFloch, M. D. Thanh, A Godunov-type method for the shallow water equations with discontinuous topography in the resonant regime, Journal of Computational Physics 230 (20) (2011) 7631–7660.

[33] A. I. Aleksyuk, V. V. Belikov, The uniqueness of the exact solution of the Riemann problem for the shallow water equations with discontinuous bottom, Journal of Computational Physics 390 (1) (2019) 232–248.